Docking and DFT analysis of organic 3-methyl salicylic acid

M. Govindarajan[a,*],

[a]*Department of Physics, Avvaiyar Government College for Women (AGCW),Karaikal , Puducherry 609 602, India*

[b]*Arignar Anna Government Arts and Science College for Women (AAGASC),Karaikal Puducherry 609602, India*

Abstract

In this work, the experimental and theoretical on the structure of the molecule was studied. The conformational analysis was used through the potential surface scan in order to determine the most optimized geometry of the 3-methyl salicylic acid molecule (3MESA).The FT-IR and FT-Raman spectra were recorded. The molecular geometry and vibrational frequencies in the ground state were calculated by using the Hartree-Fock (HF) and density functional theory (DFT) methods (B3LYP) with 6-311++G(d,p) basis set. Comparison of the observed fundamental vibrational frequencies of 3MESA with calculated results by HF and DFT indicates that B3LYP is excellent to HF method for molecular vibrational problems. The deviations between the observed and calculated wavenumber values are very small. The theoretically calculated FT-IR and FT-Raman spectra of the title molecule have been constructed. A study on the electronic properties, such as HOMO, HOMO-1, LUMO and LUMO+1 energies were performed by this molecule. Molecular electrostatic potential (MESP) and thermodynamic properties were performed. The molecular docking activity is available in target amino acids and the analysis is for both anticipating and analyzing the molecular mechanisms of ligand recognition. Mulliken atomic charges of 3MESA was calculated and compared with molecule. Natural bond orbital analysis (NBO) has been carried out to explain the charge transfer or its delocalization due to the intra-molecular interaction among bonds.

Keywords: Vibrational spectra; 3-methyl salicylic acid; HF and DFT calculations; HOMO-LUMO.

1. Introduction

3-Methylsalicylic acid is chemical compound with the chemical formula $CH_3C_6H_3$ (CO_2H) (OH). It is a white solid that is soluble in basic water and in polar organic solvents. At neutral pH, the acid exists as 3-methylsalicylate and functional groups include a carboxylic acid and a phenol group [1]. It is one of four isomers of methyl salicylic acid. It acid was used in the synthesis of 8-methyl-2-thioxo-2,3-dihydro-4H-1,3-benzoxazin-4-one,7-hydroxy-8-methyl-2-thioxo-2,3-dihydro-4H-1,3-benzoxazin-4-one, (R)-, (S)- and (RS)-hydroxymethylmexiletine [2]. The microwave (MW) spectra of the simpler of these compounds, that is formic [3], acetic [4], propionic [5], benzoic [6] and cyclopropanecarboxylic acids [7], are dominated by the Z-COOH conformation (trans arrangement of the hydrogen atoms) of the carboxylic group.

Salicylic acid is extensively used in agriculture, drugs, cosmetics and as intermediate in the synthesis of fine chemicals. In agriculture, it serves as a plant growth regulator [8] and an elicitor to create resistive materials against plant pathogens [9]. It has obvious effect on the fruit ripening, freshness of horticultural product and seed germination [10]. In the pharmaceutical field, salicylic acid is the main raw material for the synthesis of non-steroidal anti-inflammatory drug, aspirin [11]. It is also used in the removal of excessive keratin in hyperkeratotic skin disorders in cosmetics [12]. In addition, the salts of SA and SA derivatives are also extensively used in pharmaceutical field and industry, for example, bismuth subsalicylate can be used in the treatment of acute diarrhea in children [13] and indigestion [14] Ca(II) and Zn(II) alkyl salicylates can be used as lubricant additives [15].

2. Experimental details

The compound under investigation namely 3MESA is purchased from M/S Aldrich Chemicals, (USA) with spectroscopic grade and it is used as such without any further purification. The FT-IR spectrum of the compound was recorded in Perkin-Elmer 180 Spectrometer between 4000–100 cm^{-1}. The spectral resolution is ± 2 cm^{-1}.

The FT-Raman spectrum of the compound was also recorded in the same instrument with FRA 106 Raman module equipped with Nd: YAG laser source operating at 1.064 μm line widths with 200 mW powers. The spectra were recorded with scanning speed of 30 cm^{-1} min^{-1} of spectral width 2 cm^{-1}. The frequencies of all sharp bands are accurate to ± 1 cm^{-1}.

UV–Vis spectra of the title molecule were registered in the range of 200–400 nm by using Shimadzu UV-2101 PC, UV–Vis recording Spectrometer, solved in DMSO.

3. Quantum chemical calculations

The quantum chemical calculations have been fitted at HF and DFT (B3LYP) methods with 6-311++G(d,p) basis sets using the Gaussian 09W program [16]. The optimized molecule parameters have been evaluated for the calculations of vibrational frequencies by assuming Cs point group symmetry. At the optimized geometry for the title molecule no imaginary frequency modes were obtained, therefore there is a true minimum on the potential energy surface was found. As a result, the unscaled calculated frequencies, infrared intensities, Raman activities and depolarization ratios are obtained. In order to fit the theoretical wavenumbers to the experimental, the scaling factors have been introduced by using a least square optimization of the computed to the experimental data. Vibrational frequencies are scaled as 0.9067 for HF and the range of wavenumbers above 1700 cm^{-1} are scaled as 0.958 and below 1700 cm^{-1} scaled as 0.983 for B3LYP [17] to account for systematic errors caused by basis set incompleteness, neglect of electron correlation and vibrational anharmonicity. After scaled with the scaling factor, the deviation from the experiments is less than 10 cm^{-1} with a few exceptions. The assignments of the calculated normal modes have been made on the basis of the corresponding PEDs. The PEDs are computed from quantum chemically calculated vibrational frequencies using VEDA program [18]. Gauss view program [19] has been considered to get visual animation and for the verification of the normal modes assignment.

The electronic absorption spectra for optimized molecule calculated with the time dependent DFT (TD-DFT) at B3LYP/6-311++G(d,p) level in gas phase and solvent (acetonitrile, chloroform, DMSO and ethanol). The changes in the thermodynamic functions (the heat capacity, entropy, and enthalpy) were investigated for the different temperatures from the vibrational frequency calculations of title molecule.

4. Results and discussion

4.1. Potential energy scan

A potential energy scan is mainly used to describe the relationship between potential energy and molecular geometry. The conformational analysis was used through the potential surface scan in order to determine the most optimized geometry of the 3MESA molecule. The first potential energy scan curve is re carried out with dihedral angles C6-C10-O2-H5 the link between the phenyl ring and oxygen hydrogen group, respectively. During the scan, all the geometrical parameters were simultaneously relaxed and were varied in steps of 30° from 0 to 360°. The curve of the potential energy as a function of the dihedral angle was presented in Fig 1. In this, the minimum energy would be equal to -0.181863 hartree and the optimized structure was equivalent that energy. .One conformer is obtained out of 11 conformers. The energies of the conformers of the 3MESA molecule were calculated by AM1 theory.

The structure optimization of the 3MESA molecule with B3LYP/6-311++G (d,p) basis sets is approximately -535.5152 a.u. But, the HF/6-311++G (d,p) method the energy becomes -532.3539 a.u. The difference between the energy is about 3 a.u. The zero point energies are also in the same trend of the global minimum energy. The global minimum energy values were observed at 91.8928 and 98.7468 in the B3LYP/6-311++G (d,p) and HF/6-311++G(d,p).

4.2. Molecular geometry

3MESA is substituted aniline with three different functional groups; a hydroxyl bond (OH), methyl group and acid (COOH) group in a benzene ring. The optimized geometry of 3MESA which performed by HF and B3LYP methods with atoms numbering is shown in Fig. 2. The optimized bond lengths and bond angles of title compound are given in Table 1. From Table 1, it is found that bond angles and dihedral angles given by DFT/B3LYP method are equal with those by HF method, but the bond lengths calculated by HF method are little closer than those by DFT/B3LYP method. The ring appears little distorted and angles slightly out of perfect hexagonal structure. In this work, geometry optimization parameters for 3MESA have been employed without symmetry constrain. The bond lengths HF are slightly better than the B3LYP geometry. The agreement for bond angles is not as good as that for the bond distances.

The carbon atoms are bonded to the hydrogen atoms with σ bond in benzene. The ring carbon atoms in substituted benzenes exert a larger attraction on the valence electron cloud of the hydrogen atom resulting in an increase in the C–H force constant and a decrease in the corresponding bond length. The reverse holds well on substitution with electron donating groups. The actual change in the C–H bond length would be influenced by the combined effects of the inductive–mesomeric interaction and the electric dipole field of the polar substituent. The average bond distances of C-C and C-H in the benzene ring calculated by HF method are 1.0698 and 1.0699 Å, respectively.

The bond lengths of C–C bond are almost same in value, which is due to the substitutions on the benzene ring in the place of acid and methyl group. The optimized CH_2 (methyl group) bond length are calculated 0.3604, 0.3696 and 0.9361 Å by HF and 0.6418 and 1.1002 Å by B3LYP with 6-311++G(d,p) method. The optimized C-O bond length by two methods is 1.3910, 1.2075 and 1.3620 Å or B3LYP/6-311+G(d,p) and 1.4299, 1.2583 and 1.4299 Å for HF/6-311+G(d,p) methods, respectively. The C-O bond length is shorter B3LYP than HF values. The O-H bond length indicates a considerable decrease when substituted in place of C-H. In this study, the O-H bond lengths also are lesser than the C-H ones. The O-H bond lengths vary from 0.9925 to 0.9936 Å and from 0.8531 to 0.8441 Å by B3LYP and HF methods, respectively.

The asymmetry of the benzene ring is also evident from the positive deviation of C7–C8–C9, C8–C9–C6 and C4-C5-C6 angles which are calculated ca. 120.28°, 120.58° and 120.51° (B3LYP) and negative deviation of the remaining angles from the normal value of 120° (for example the C4-C7-C9 angle found to be bigger and C5-C6-C8 angle found to be smaller than hexagonal angles). The angles of O3-C10-O2 are calculated as 118.01° and 119.05° by B3LYP and HF methods.

4.3. Thermodynamic Properties

The values of thermodynamic parameters of 3MESA at 298.15 K in ground state are listed in Table 2. On the basis of vibrational analysis, the statically thermodynamic functions: heat capacity (C), entropy (S), and enthalpy changes (ΔH) for the title molecule were obtained from the theoretical harmonic frequencies and listed in Table 4. From the Table 4, it can be observed that these thermodynamic functions are increasing with temperature between from 100 to 700 K due to the fact that the structural vibrational intensities increase with temperature [20]. The correlation equations between heat capacity, entropy, enthalpy changes and temperatures were fitted by quadratic formulas and the corresponding fitting factor (R^2) for these thermodynamic properties is determined. The corresponding fitting equations are as follows and the correlation graphics of that show in Figs. 3.

$$C = -1.85243 + 0.15265T - 7.82243 \times 10^{-5}T^2 \quad (R^2 = 0.99834)$$

$$S = 46.8553 + 0.21112T - 1.45006 \times 10^{-4}T^2 \quad (R^2 = 0.99357)$$

$$H = -0.78236 + 0.01198T + 4.21846 \times 10^{-5}T^2 \quad (R^2 = 0.99927)$$

All the thermodynamic data supply helpful information for the further study on the 3MESA. They can be used to compute the other thermodynamic energies according to relationships of thermodynamic functions and estimate directions of chemical reactions according to the second law of thermodynamics in Thermochemical field. Notice: all thermodynamic calculations were done in gas phase and they could not be used in solution.

4.4. Mulliken atomic charges

Mulliken atomic charge calculation has an essential role in the application of quantum chemical application to molecular system because of atomic charges effect dipole moment, molecular polarizability, electronic structure and a lot of properties of molecular systems. The mulliken charge distributions over the atoms suggest the formation of donor and acceptor pairs giving the charge transfer in the molecule. The mulliken population analysis in 3MESA molecule was calculated using B3LYP and HF levels with 6-311++G(d,p) basis sets and are listed in Table 3 and are shown in the Fig 4. The results show that substitution of the aromatic ring by
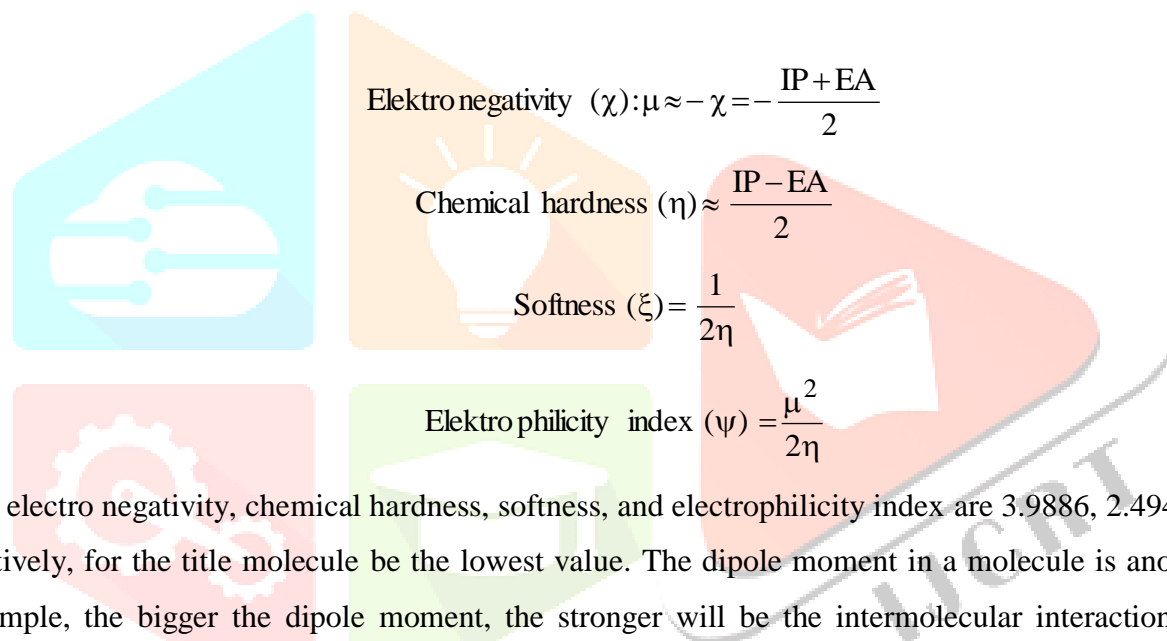
COOH and OH group of atoms leads to a redistribution of electron density. The charge changes with basis set presumably occurs due to polarization. For example, the charge of C (10) atom is 0.630878 e⁻ for B3LYP/6-311++G(d,p) and 0.507018 e⁻ for HF/6-311++G(d,p). The charge distribution of 3MESA (Fig. 6) shows all the hydrogen atoms and carbon atoms in few sets are positively charged, whereas the magnitudes of the carbon atomic charges for the compounds were found to be both positive and negative at the basis set. The charge of O (1) is negative in all basis set, however the value -0.173309 e⁻ in B3LYP method with 6-311++G(d,p) is observed. The charge of the oxygen atom -0.288135 e⁻ is in HF/6-311++(d,p). The COOH and OH group in the molecule accepted the electrons.

4.5. Frontier molecular orbitals (FMOs)

The FMO play an important role in the optical and electric properties, as well as in quantum chemistry and UV–Vis. spectra [21]. Gauss-Sum 2.2 Program [22] was used to calculate group contributions to the molecular orbitals (HOMO and LUMO). The HOMO represents the ability to donate an electron, LUMO as an electron acceptor represents the ability to obtain an electron. The energy gap between HOMO and LUMO determines the kinetic stability, chemical reactivity and, optical polarizability and chemical hardness–softness of a molecule. The hard molecules are not more polarizable than the soft ones because they need big energy to excitation.

In order to evaluate the energetic behavior of the title compound, we carried out calculations in acetonitrile, chloroform, DMSO, ethanol and gas phase. The energies of four important molecular orbitals of 3MESA: the second highest and highest occupied MO's (HOMO and HOMO−1), the lowest and the second lowest unoccupied MO's (LUMO and LUMO+1) were calculated using B3LYP/6-311++G(d,p) and are presented in Table 4. 3D plots of the HOMO-1, HOMO, LUMO and LUMO+1 orbitals computed at the B3LYP/6-311G++(d,p) level for 3MESA molecule (in gas phase) are illustrated in Fig. 5. It is clear from the figure that, while the HOMO is localized on almost the whole molecule, LUMO is especially localized on the ring. Both the HOMOs and the LUMOs are mostly -anti-bonding type orbitals. The calculated energy values of the HOMO are --6.6242, -6.6006, -6.4832 and -6.6220 eV in acetonitrile, chloroform, DMSO and ethanol, respectively. Similarly, the LUMO energy values are -1.7242, -1.6729, -1.4940 and -1.7201 eV. The energy gap between HOMO and LUMO indicates the molecular chemical stability. In this molecule, the value of energy separation between the HOMO and LUMO are 4.9000, 4.9277, 4.9892 and 4.9019 eV in acetonitrile, chloroform, DMSO and ethanol, respectively. The major contributions of the transitions were designated with the aid of SWizard program [23]. In view of calculated absorption spectra, the maximum absorption wavelength corresponds to the electronic transition from the HOMO to LUMO.

The other wavelength, excitation energies, oscillator strength and calculated counterparts with major contributions can be seen in Table 5. The electronic properties of the molecules are calculated from the total energies and the Koopmans' theorem. The ionization potential is determined from the energy difference between the energy of the compound derived from electron-transfer (radical cation) and the respective neutral compound; $IP = E_{cation} - E_n$; $IP = -E_{HOMO}$ while the electron affinity is computed from the energy difference between the neutral molecule and the anion molecule: $EA = E_n - E_{anion}$; $EA = -E_{LUMO}$, respectively. The other important quantities such as electronegativity (χ), hardness (η), softness (ζ), and electrophilicity index (ψ) were deduced from ionization potential and electron affinity values [30-32].

$$\text{Elektro negativity } (\chi): \mu \approx -\chi = -\frac{IP + EA}{2}$$

$$\text{Chemical hardness } (\eta) \approx \frac{IP - EA}{2}$$

$$\text{Softness } (\xi) = \frac{1}{2\eta}$$

$$\text{Elektro philicity index } (\psi) = \frac{\mu^2}{2\eta}$$

The values of electro negativity, chemical hardness, softness, and electrophilicity index are 3.9886, 2.4946, 0.2004 and 3.1886 eV in DMSO, respectively, for the title molecule be the lowest value. The dipole moment in a molecule is another important electronic property. For example, the bigger the dipole moment, the stronger will be the intermolecular interactions. The calculated dipole moment values for the molecules are also given in Table 5. Based on predicted dipole moment values, it is found that, in going to the DMSO 4.0268 D, the dipole moment value increases (Table 5).

4.6. Ultraviolet spectra analysis

Ultraviolet spectra analyses of 3MESA have been investigated in DMSO chloroform and gas phase by theoretical calculation. On the basis of fully optimized ground-state structure, TD-DFT/B3LYP/6-311++G(d,p) calculations have been used to determine the low-lying excited states of 3MESA. The theoretical electronic excitation energies, oscillator strengths and absorption wavelength are also listed in Table 5 and the UV graph of solvents are shown in the Fig 6. Calculations of the molecular orbital geometry show that the absorption maxima of this molecule correspond to the electron transition between frontier orbitals such as translation from HOMO to

LUMO. As can be seen from Table 5, the calculated absorption maxima values have been found to be 284, 262 and 250 nm for gas phase, 289.23, 254.16, 237.16, 221.25 and 208.36 nm for acetonitrile, 287.93, 257.14, 236.55, 223.76 and 210.16 nm for chloroform, 283.33, 254.83, 231.86, 203.10 and 194.10 nm for DMSO and 2893.18, 254.41, 237.16, 221.42 and 208.50 nm for ethanol at DFT/B3LYP/6-311++G(d,p) method. It is seen from Table 5, calculations performed at DMSO and chloroform are close to each other when compared with gas phase and also the absorption maxima values of gas phase are larger than that of the organic solvents.

4.7. Electrostatic potential, total electron density and molecular electrostatic potential

In the present study, the electrostatic potential (ESP), total electron density (ED) and molecular electrostatic potential (MEP) of 3MESA are illustrated in Fig. 7. The MEP which is a plot of electrostatic potential mapped onto the constant electron density surface. The MEP is a useful property to study reactivity given that an approaching electrophile will be attracted to negative regions (where the electron distribution effect is dominant). In the majority of the MEP, while the maximum negative region which preferred site for electrophilic attack indications as red colour, the maximum positive region which preferred site for nucleophilic attack symptoms as blue colour. The importance of MEP lies in the fact that it simultaneously displays molecular size, shape as well as positive, negative and neutral electrostatic potential regions in terms of colour grading (Fig. 7) and is very useful in research of molecular structure with its physiochemical property relationship [24-26]. The resulting surface simultaneously displays molecular size and shape and electrostatic potential value.

The different values of the electrostatic potential at the MEP surface are represented by different colors; red, blue and green represent the regions of most negative, most positive and zero electrostatic potential, respectively. The color code of these maps is in the range between -0.06581 a.u. (deepest red) to 0.06581 a.u. (deepest blue) in compound, where blue indicates the strongest attraction and red indicates the strongest repulsion. Regions of negative V(r) are usually associated with the lone pair of electronegative atoms. As can be seen from the MEP map of the title molecule, while regions having the positive potential are over the hydrogen atoms, the regions having the negative potential are over the electronegative (COOH and OH) atoms.

4.8. Vibrational analysis

The maximum number of potentially active observable fundamentals of a non-linear molecule which contains N atoms is equal to (3N-6), apart from three translational and three rotational degrees of freedom. Hence, 3MESA molecule, that was planar, has 19 atoms with 51 normal modes of vibrations. All vibrations are active both in Raman and infrared absorption. The detailed vibrational assignment of the experimental wavenumbers is based on normal mode analyses and a comparison with theoretically scaled wavenumbers by B3LYP and HF methods. The observed and simulated infrared and Raman spectra of 3MESA is shown in Figs. 8-9,

respectively. The observed and scaled theoretical frequencies using HF and DFT (B3LYP) with 6-311++G(d,p) basis sets with PEDs are listed in Table 6.

4.8.1. C-H vibrations

The aromatic C–H stretching vibrations in tetra substituted benzene rings are generally observed in the region 3000–3100 cm^{-1} [34]. They are not appreciably affected by the nature of the substituents [27-29]. A very weak band is observed at 3080 and 3030 cm^{-1} in FT-Raman can be assigned to C-H stretching with PEDs 99% and 98%, respectively. Two aromatic CH stretching band is found to be weak and this is due to the decrease of dipole moment caused by the reduction of negative charge on the carbon atom. This reduction occurs because of the electron withdrawal on the carbon atom by the substituent due to the decrease of inductive effect. The corresponding calculated fundamentals using B3LYP/6-311++G(d,p) are 3086, 3055 and 3030 cm^{-1}. These deviations have been reduced by the scaling procedure and scaled wave numbers.

The bands due to C–H in-plane bending vibrations are observed in the region 1000–1300 cm^{-1}[30,31] . For this compound, the C–H in-plane bending vibrations were observed at 1175 and 1168 cm^{-1} in FT-IR and at 1105 cm^{-1} in FT-Raman. The PED of vibrations shows that they are not in pure modes. The theoretically scaled vibrations by B3LYP/6-311++G(d,p) level method also shows good agreement with experimentally recorded data. The C–H out-of-plane bending vibrations appear within the region 900–675 cm^{-1}. But, they the vibrations identified at 458 cm^{-1} in FT-IR and 390 and 350 **cm^{-1}** in FT-Raman are assigned to C–H out-of-plane bending for 3MESA. After scaling procedure, the theoretical C–H vibrations are in slightly higher values with the experimental values and literature.

4.8.2. Ring vibrations

The ring stretching vibrations are significant in spectrum analysis of benzene and its derivatives. The C=C and C-C stretching vibrations, known as semicircle stretching usually occur in the region 1400–1625 cm^{-1} [32, 33]. The C=C stretching vibrations of the present compound are strongly observed at 1485, 14470 and 1430 cm^{-1}. These assignments are in line with the literature. The C-C stretching vibrations were observed at 1390, 1336 and 1325 cm^{-1}. When compared to the literature range cited above, there is a considerable decrease in frequencies which is also worsening with the increase of mass of substitutions.

In the present work, three bands present at 680 and 620 cm^{-1} assigned to CCC in-plane bending and no supplementary bands assigned to CCC out-of-plane bending. These assignments are in line with the assignments proposed by the literature. The theoretically computed values by B3LYP/6-311++G(d,p) method for CCC out-of-plane bending are shown in the table 6.

4.8.3. Methyl group vibrations

The compounds under investigation possess a CH_3 group at the substitution. For the assignments of CH_3 group frequencies one can expect that nine fundamentals can be associated to CH_3 group. The C-H stretching is at lower frequencies than those of the aromatic ring. The asymmetric stretch is usually at higher wavenumber than the symmetric stretch. Usually the symmetrical bands are sharper than the asymmetrical bands. Methyl group vibrations are generally referred to as electron-donating substituent in the aromatic rings system, the asymmetric C–H stretching mode of CH_3 is expected around 2980 cm^{-1} and CH_3 symmetric stretching is expected at 2870 cm^{-1} [34-37]. In 3MESA, the modes appear at 2980 and 2920 cm^{-1} in FTIR (CH_3 asymmetric stretching) and at 2870 cm^{-1} in FT-Raman (CH_3 symmetric stretching) are assigned CH_3 stretching modes of vibrations. The theoretically scaled values by B3LYP/6-311++G(d,p) method at 2980, 2915 and 2875 cm^{-1} are in good agreement with the experimental values. The asymmetric and symmetric deformation vibrations of methyl group appear within the region 1465-1440 cm^{-1} and 1390- 1370 cm^{-1} [38]. In the present investigation, the bands at 1090 and 1040 cm^{-1} in FT-IR, 965 cm^{-1} in FT-Raman with very strong intensities are observed as CH_3 asymmetric deformation and symmetric deformation vibrations for 3MESA. The methyl rocking mode vibration usually appears within the region 330, 298 and 260 cm^{-1} [35-37]. With reference to literature data, the observed bands at 1045 and 1038 cm^{-1} are assigned to out-of-plane CH_3 rocking vibrations for 3MESA.

4.8.4. COOH vibrations

Generally carboxylic acid group containing molecule possesses dimeric character. The carboxylic acid dimer is formed by strong hydrogen bonding interaction in the solid state. Hence the derivatives of carboxylic acids are best characterized by the carbonyl and hydroxyl groups. The presence of carbonyl group is the most important in the infrared spectrum because of its strong intensity of absorption and high sensitivity toward relatively minor changes in its environment. Two bands arising from C-O stretching and O-H bending appear in the spectra of carboxylic acids near 1210-1320 cm^{-1} and 1400-1440 cm^{-1}, respectively [36]. Both these bands involve some interaction between C-O stretching and in-plane C-O-H bending. In our study, the strong band at 1720 cm^{-1} and 1630 cm^{-1} are due C-O stretching in FT-IR and FT-Raman spectra respectively. The intermolecular hydrogen bonding between 3MESA molecules can significantly affect the IR spectra. The O-H stretching is characterized by a broad band appearing near about 3400 cm^{-1} [37, 38]. When the O-H in carboxylic acid do not form intramolecular bond, the stretching mode is to be expected at 3620 cm^{-1} . In the case of the O-H group forms a hydrogen bond, the OH stretching fundamental undergoes a large frequency shift, the magnitude of which reflects the strength of the hydrogen bond formed. The high strength of hydrogen bonds between the –COOH groups is reflected in a large decrease in the frequency of the O-H and C=O stretching vibrations and it is interpreted on the basis of larger

contribution from the polar resonance structure. In the present study, the computed O-H and C=O stretching vibrations for monomer are 3612 cm^{-1} and 1720 cm^{-1} , The carboxylic acid dimer has six intermolecular vibrational modes appear with other modes.

In this study, the calculated O-H stretching mode is assigned at 3620 cm^{-1} for 3MESA monomer. The medium bands observed at 1260 cm^{-1} in FT-IR spectra are probably due to the O-H in-plane bending vibration. The carboxylic acids also show the out-of-plane bending band of O-H near 750 cm^{-1}. These bands were assigned in terms of various fundamentals, overtone and combination vibrations.

4.9. Natural bond orbital (NBO) analysis

Natural bond orbital analysis (NBO) has been carried out to explain the charge transfer or its delocalization due to the intra-molecular interaction among bonds. It also provides a convenient basis for investigating charge transfer or conjugative interaction in molecular systems. The intramolecular interactions are formed by the orbital overlap between σ(C-C), σ^*(C-C), π(C-C) and π^*(C-C) bond orbitals leading to intramolecular charge transfer and cause stabilization of the system. These interactions are observed as increase in the electron density (ED) of the C-C anti-bonding orbital that weakens the respective bonds. These intermolecular charge transfer ($\sigma \rightarrow \sigma^*$, $\pi \rightarrow \pi^*$) can induce large nonlinearity of the molecule.

The strong intermolecular hyper-conjugation interactions of the σ and π electrons of the C-C bond to the anti C-C, C-H, O-C and O-H bonds lead to stabilization of some parts of the aromatic rings in the title molecule as evident from Table 2. NBO analysis has been performed on the 3MESA molecule at the B3LYP/6-311G (d,p) level in order to elucidate its intramolecular hyper-conjugation, re-hybridization and delocalization of electron density within the molecule. The strong intramolecular hyper-conjugative interactions of the σ electron of C4–C7 distributed to the σ^*(O1–C5), C4–C5, C4–C16, C7–C9, C7-H11 and C9–H13 of the ring. On the other hand, the π (C4–C7) in the ring conjugated to the anti-bonding orbital of π^*C5–C6, π^*C8–C9, π^*C16-H17 and π^*C16-H18 with the energies 0.42023, 0.29980 and 0.01213kcal/mol.

The π(C8-C9) bond is interacting with π^*(C4-C7) and π^*(C5-C6) with the energies of 0.34098 kcal/mol and 0.42023 kcal/mol for the 3MESA molecule. The σ(O1–C5) bond is contributing energy of 0.03754 , 0.01651 , 0.03069 and 0.02023kcal/mol with σ^*(C4–C5), (C4–C7), (C5–C6) and (C6–C8). Similarly, the σ(O3–C10) bond is contributing energy by 0.06272, 0.01704 and 0.03754 kcal/mol with σ^*(C6–C8), (C6–C10 and (C5–C6). LP1 of O1 is interacting with C4-C5 with the energy of 0.03754 kcal/mol only. Similarly, LP1 of O2 is contributing O3-C10 and C8-C9 and O3 is contributing O2-C10 and C6-C10 with energies of 0.01704, 0.01563 and 0.10987, 0.06272 kcal/mol.

4.10. Molecular docking

Molecular docking is a role in drug analysis for the discussion of many problematic diseases. This analysis is for both anticipating and analyzing the molecular mechanisms of ligand recognition and specificity [39, 40]. This technique provides insight into probable protein-ligand interactions and identifies the binding affinity of molecules which can a corroborate the experimental result. Here, we check the anti-psychotic activity of 3MESA molecule. The docking modeling was done using the AutoDock 4.2 package software with the target protein dopamine receptor (PDB code: 3AX7) was downloaded rom the RCSB protein data bank. For molecular docking protein was prepared by the following steps: (i) All water molecules were removed (ii) hydrogen atoms and Kollman's charges were added iii) Docked co-ligand was removed from the protein. The docking results were evaluated by sorting the docked conformations according to their predicted binding free energy. The protein-ligand nteraction complex is given in Fig. 10, displaying the 3MESA conformer with the best predicted binding free energy. Visual analysis of 3MESA showed that the whole ligand was focused on the groove of the protein. The 3MESA was docked deeply with the binding pocket of 3AX7 forming the hydrogen bonds with THP2, GLN62, LYS165, PRO224, GLY528, ASP571, ALA876, GLY868, SER870, APS872, ASN908, THR909, LYS1326, XAY3003 and BCT1337. The grid dimensions are 49.3, 56.3 and 55.6 along x, y and z dimension. The dielectric value may be up to 24.78.

5.   Conclusion

The vibrational analysis of 3MESA are done by HF and DFT-B3LYP methods with 6-311++G(d,p) basis sets. The influences of oxygen-hydrogen, acid group and methyl group of the title compound are discussed. The observed and stimulated spectra are agreed for the good frequency fit in DFT/B3LYP/6-311++G(d, p) method. The less standard deviation between calculated and experimental wave numbers is confirmed by the qualitative agreement between the calculated and observed frequencies. The same trend is also reflected in the optimized parameters. The global minimum energy between the different methods shows the difference in optimizations between the same and the different sets. The quantum chemical calculations help us to identify the structural properties of the 3MESA molecule. The good agreement of the theoretical and observed wavenumbers is showing for better calculations. Furthermore, the thermodynamic and electronic absorption properties of the compounds have been calculated. The correlations graph between the some statistical thermodynamics factors and temperature are also obtained. It was seen that the heat capacities, entropies and enthalpies with temperature owing to the intensities of the molecular vibrations increase with increasing temperature. The charge of the oxygen atom is indicated in the molecule by accepting the electrons. Natural bond orbital analysis (NBO) has been given out to describe the charge transfer or its delocalization due to the intra-molecular interaction among bonds. The 3MESA was docked deeply

with the binding pocket of 3AX7 forming hydrogen bonds are shown.

References

[1]	T.Iijima, T.amaguchi , Applied Catalysis A. 345: 12–17(2008)

[2]	K.M. Pritchard, Synth. Commun, 35 (2), 1601-11 2005.

[3]	 V. Lattanzi, A. Walters, B.J. Drouin, J.C. Pearson, Astrophys. J. Suppl. Ser. 176
(2008) 536;

[4]	B.P. van Eijck, J. van Opheusden, M.M.M. van Schaik, E. van Zoeren, J. Mol.
Spectrosc. 86 (1981) 465;

[5]	B. Ouyang, B.J. Howard, J. Phys. Chem. A 112 (2008) 8208;

[6]	M. Onda, M. Asai, K. Takise, K. Kuwae, K. Hayami, A. Kuroe, M. Mori, H.
Miyazaki, N. Suzuki, I. Yamaguchi, J. Mol. Struct. 482/483 (1999) 301.

[7]	K.-M. Marstokk, H. Møllendal, S. Samdal, Acta Chem. Scand. 45 (1991) 37

[8]	 J.S. Jorg Durner, Daniel F. Klessig, Trends Plant Sci., 2 (7), pp. 266-274, (1997)

[9]	P.S. Nasser Yalpani, T. Michael, A. Wilson Daniel, A. Kleier, llya Raskin, Plant Cell, 3, pp. 809-818 ,(1991).

[10]	S.Y. Lee, P.N. Damodaran, K.S. Roh, Saudi J. Biol. Sci., 21, pp. 417-426, (2014).

[11]	J. O III, J. Chem. Educ., 75 (10), pp. 1261-1263, (1998).

[12]	R.K. Madan, J. Levitt, J. Am. Acad. Dermatology, 70, pp. 788-792, (2014).

[13]	A.P. Soriano-Brucher H, M. O'Ryan, Pediatrics, 87, pp. 18-27, (1991).

[14]	M.J.H.N. Francis, J. Hailey, Arch. Intern Med., 144, pp. 269-272, (1984).

[15]	D.G. Larsson, Biol. Sci., 369 (2014)

[16]	Frisch M J, Gaussion 09 Program, Gaussian, Inc., Wallingford, CT, 2004.

[17]	Karabacak M, Kurt M, Spectrochim. Acta A 71 (2008) 876-883.

[18]	Jamróz M H, Vibrational Energy Distribution Analysis, VEDA 4, Warsaw, 2004.

[19]	Dennington R I, Keith T, Millam J, Eppinnett K, W. Hovell, Gauss View Version 2003.

[20]	J Bevan Ott, J. Boerio-Goates, Calculations from Statistical Thermodynamics, Academic Press, 2000

[21]	I. Fleming, Frontier Orbitals and Organic Chemical Reactions, Wiley, London, 1976.

[22]   N.M.O' Boyle, A.L.tenderholt, K.M.langer, A Library for package-independent computational chemistry

algorithms.J.Comput.Chem. 29(2008) 839-845.

[23] S.I. Gorelsky, SWizard Program Revision 4.5, http://www.sg.chem.net/, University of Ottawa, Ottawa, Canada, 2010.

[24]   I. Alkorta, J.J. Perez, Int. J. Quant. Chem. 57 (1996) 123. 401.

[25]   E. Scrocco, J. Tomasi, in: P. Lowdin (Ed.), Advances in Quantum Chemistry, 402 Academic Press, NewYork, 1978. 403.

[26]   F.J. Luque, M. Orozco, P.K. Bhadane, S.R. Gadre, J. Phys. Chem. 97 (1993) 9380. 404.

[27]   N.B. Colthup, L.H. Daly, S.E. Wiberley, Introduction to Infrared and Raman Spectroscopy, Academic Press, New York, 1964.

[28]   G.Socrates, Infrared and Raman Characteristic Group Frequencies –Tables and   Charts. third ed., Wiley, New York, 2001.

[29]   F.R. Dollish, W.G. Fateley, F.F. Bentley, Characteristic Raman Frequencies of Organic Compounds, Wiley, New York, 1997.

[30]   G.Varsanyi, Vibrational Spectra of Benzene Derivatives, Academic Press, New York, 1969.

[31]   M.H. Jamroz, J.Cz. Dobrowolski, R. Brzozowski, J. Mol. Struct. 787 (2006) 172-183.

[32]   A. Altun, K. Gölcük, M. Kumru, J. Mol. Struct. (Theochem.) 625 (2003) 17-24.

[33]   V. Krishnakumar, R.J. Xavier. Indian J. Pure. Appl. Phys., 41 (2003) 95–98.

[34]   N.P. Singh, R.V. Yadav. Indian J. Phys. B, 75 4 (2001) 347-355.

[35]   J. Mohan, Organic Spectroscopy-Principles and Applications, Narosa Publishing House, New Delhi, 2001.

[36]   B. Karthikeyan, Spectrochim. Acta A 64 (2006) 1083-1087.

[37]   N. Sundaraganesan, S. Ilakiamani, B.D. Joshua, Spectrochim. Acta A 68 (2007) 680-687.

[38]   H. Endredi, F. Billes, G. Keresztury, J. Mol. Struct (Theochem) 677 (2004) 211-225.

[39]   P. Manjusha, Johanan Christian Prasana, S. Muthu, B. Fathima Rizwana,

Chem. Data.Coll. 20 (2019) 100191.

[40]   BR. Raajaraman, N.R. Sheela, S. Muthu, J. Mol. Struct. 1188,   (2019) 99-109.

Fig .1 Potential energy of 3MESA

Fig .2 Optimized geometry of 3MESA

Fig .3 Correlation graph of thermodynamic functions of 3MESA

Fig .4 Mulliken population analysis of 3MESA
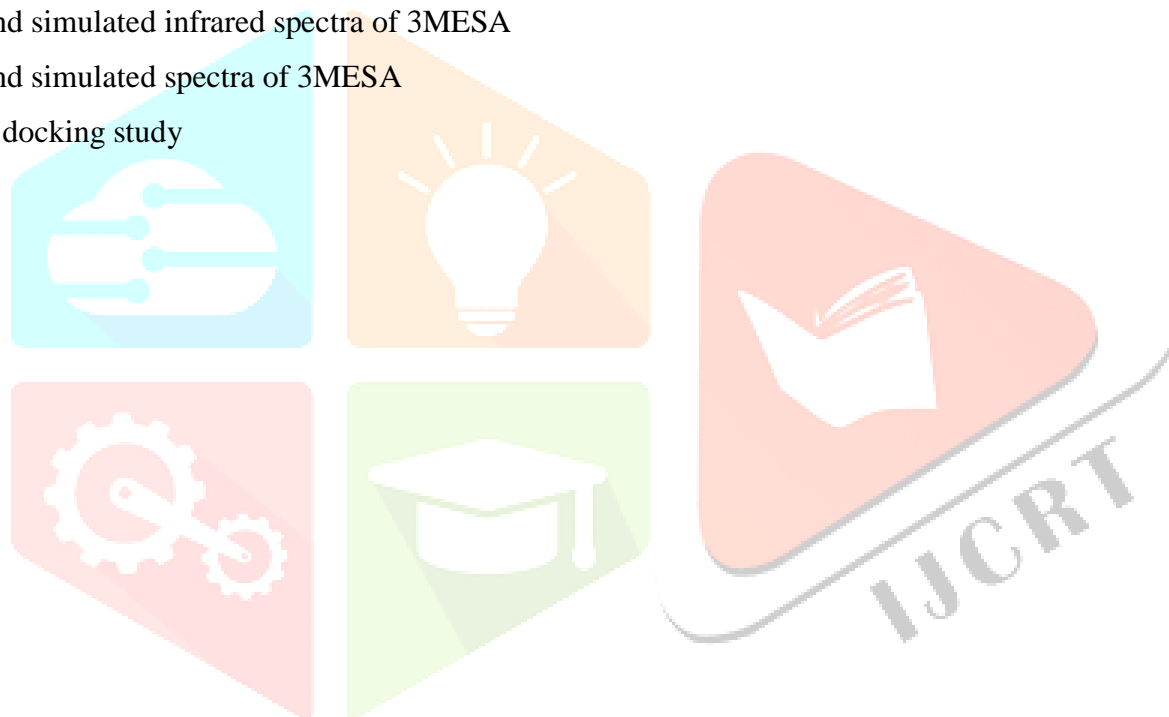
Fig .5 HOMO-1, HOMO, LUMO and LUMO+1 of 3MESA

Fig .6 UV graph of 3MESA

Fig .7 Molecular electrostatic potential (MEP) of 3MESA

Fig .8 Observed and simulated infrared spectra of 3MESA

Fig .9 Observed and simulated spectra of 3MESA
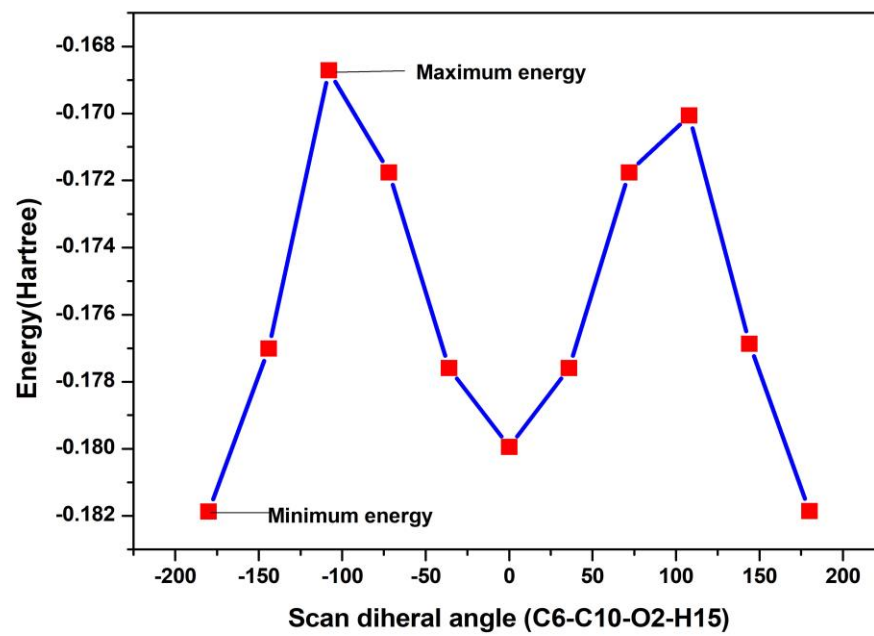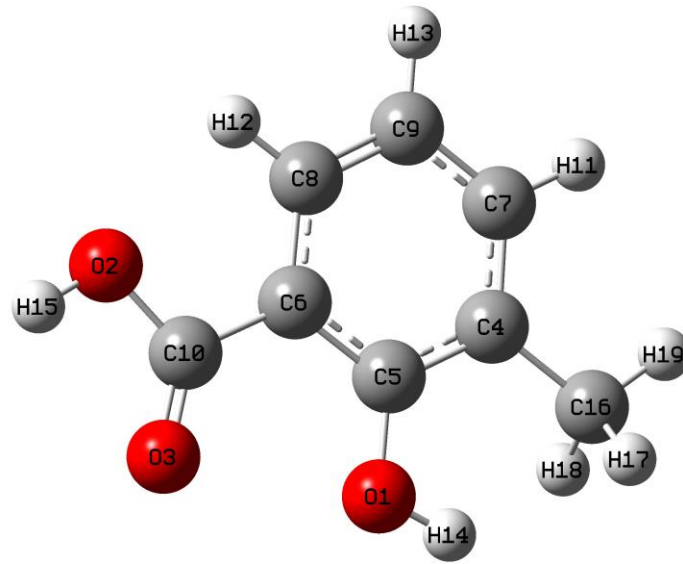
Fig.10 Molecular docking study

Fig .1

Fig .2

Fig .3

Mulliken charges   B3LYP

Mulliken charges   HF

Fig .4
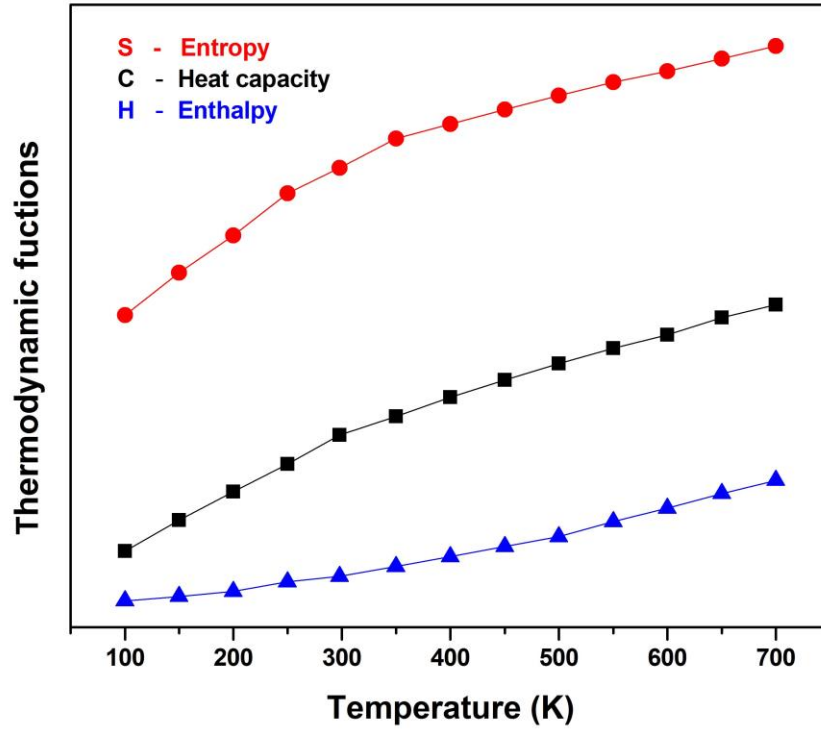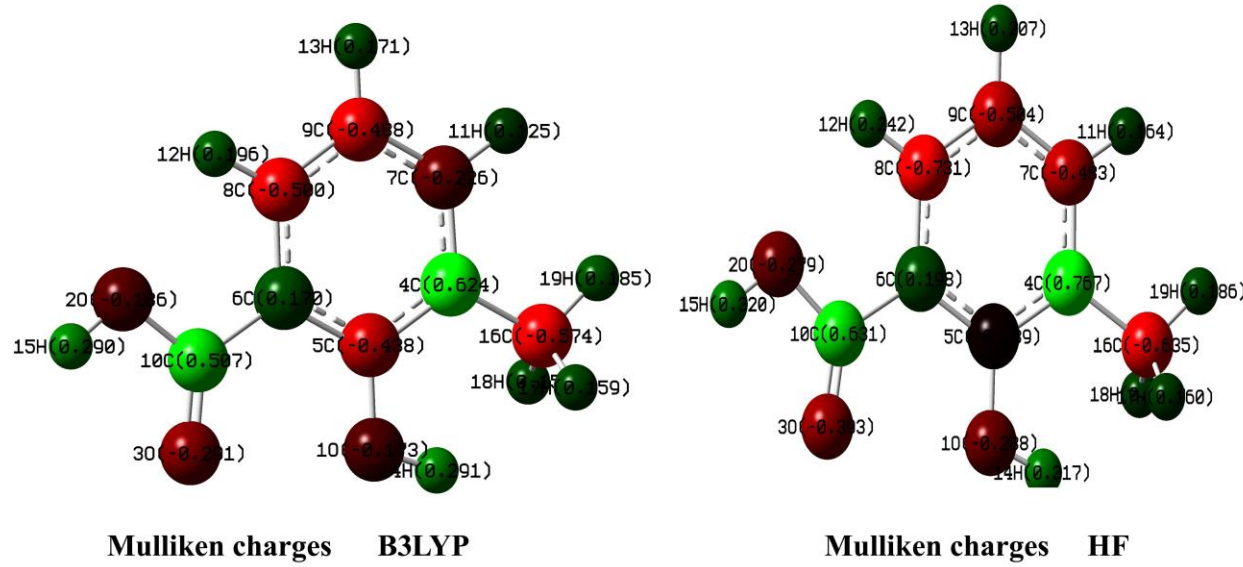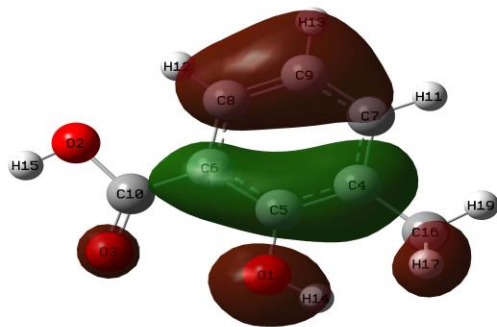
HOMO= –6.4097 eV
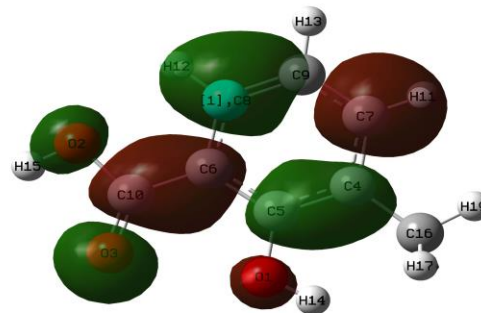
LUMO= –1.3334 eV

HOMO-LUMO=5.0762
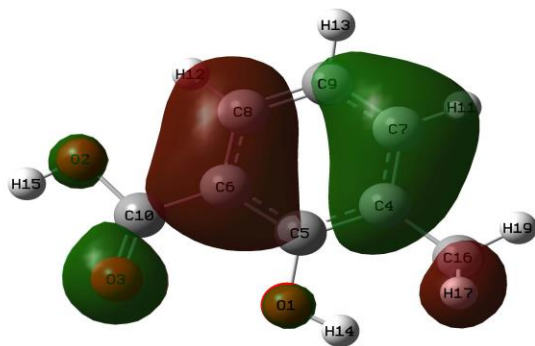
HOMO-1= –7.1778 eV
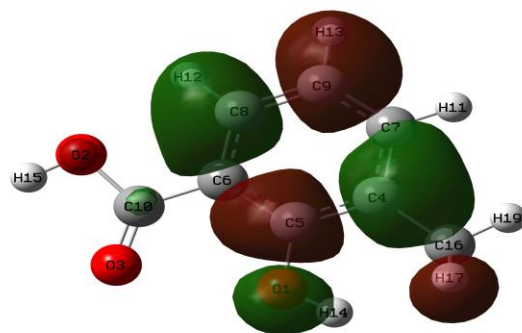
LUMO+1=-0.2098 eV

HOMO-1-LUMO+1= 6.9679 eV

Fig .6

Nucleophilic region

Electrophilic region
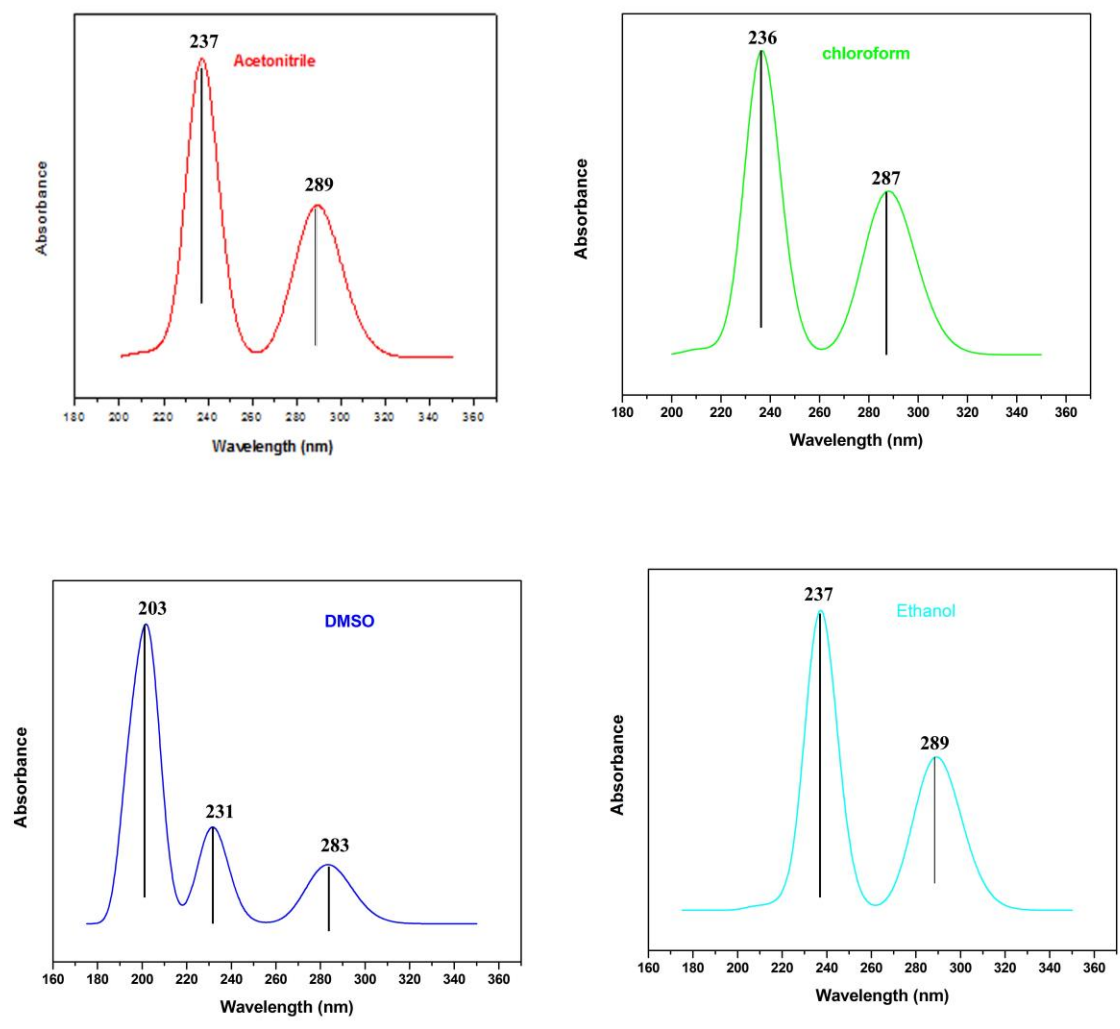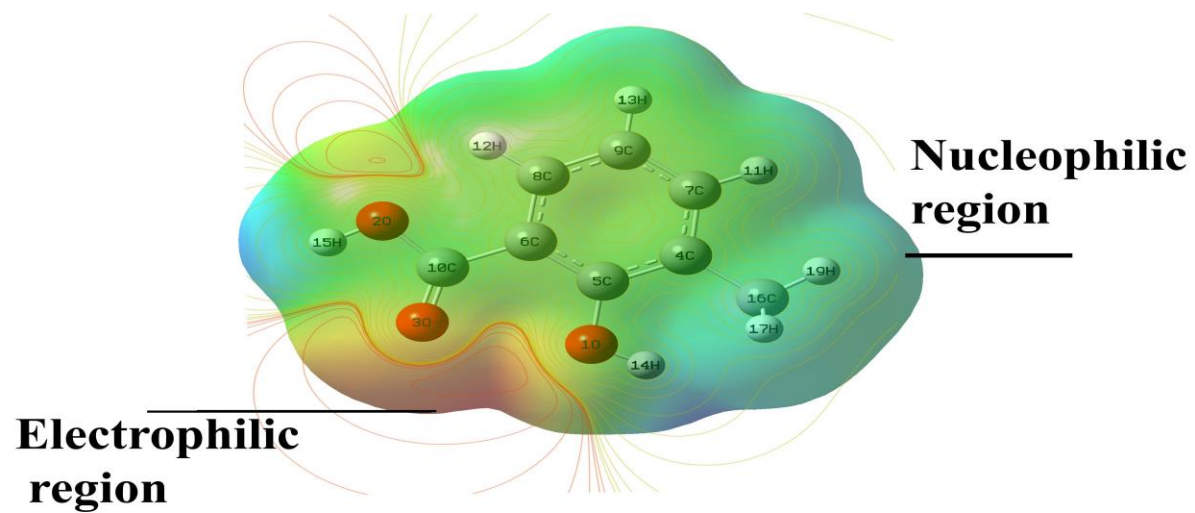
MESP = -0.06581 to +0.06581
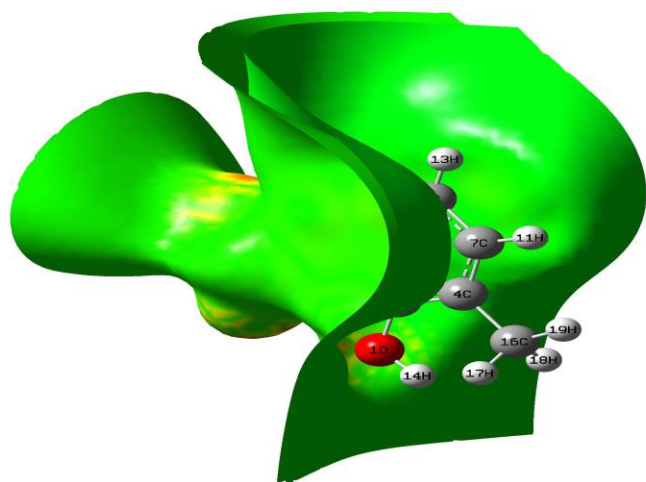
ESP = -0.01263 to +0.01263

Fig .7
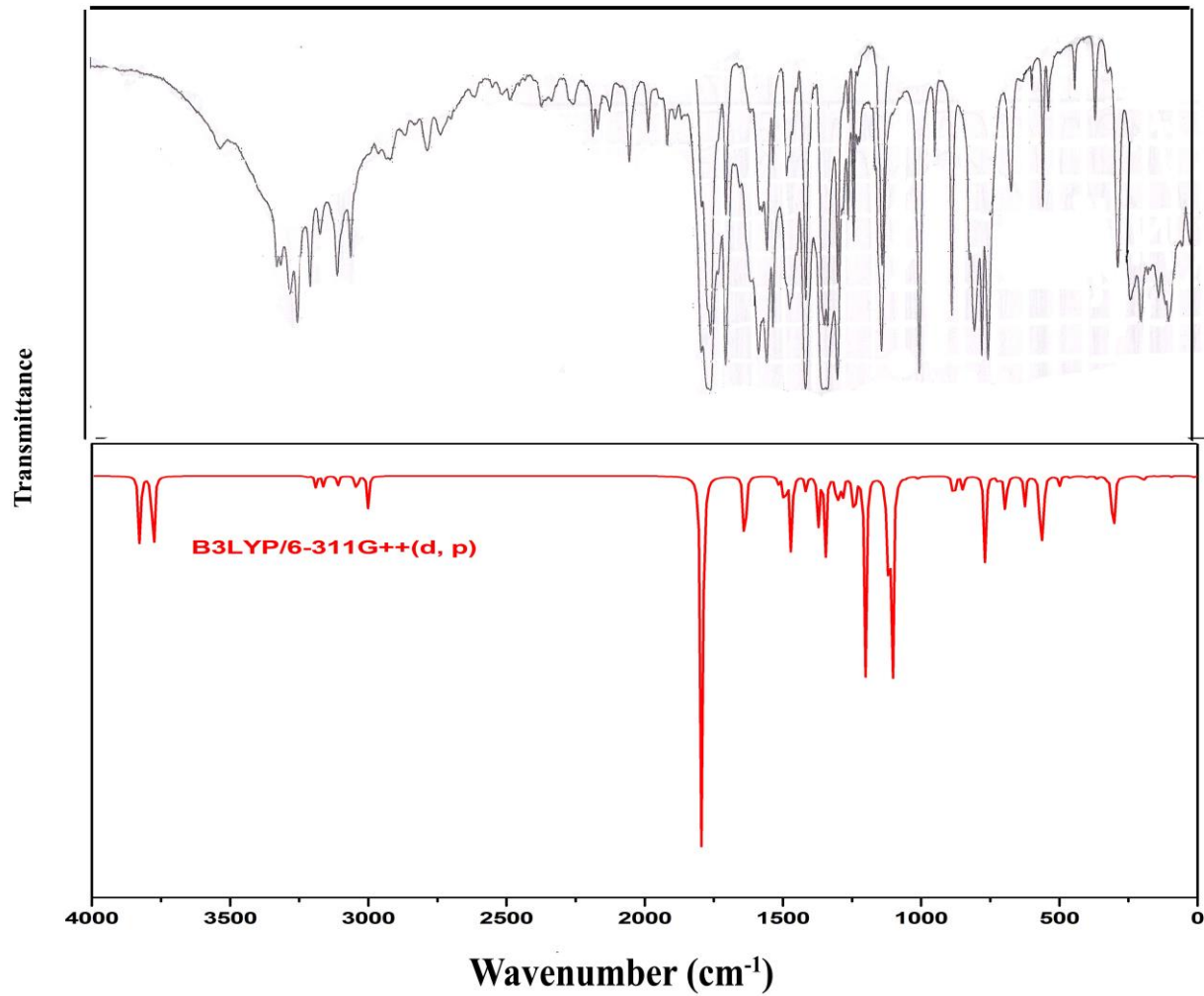
Fig .8
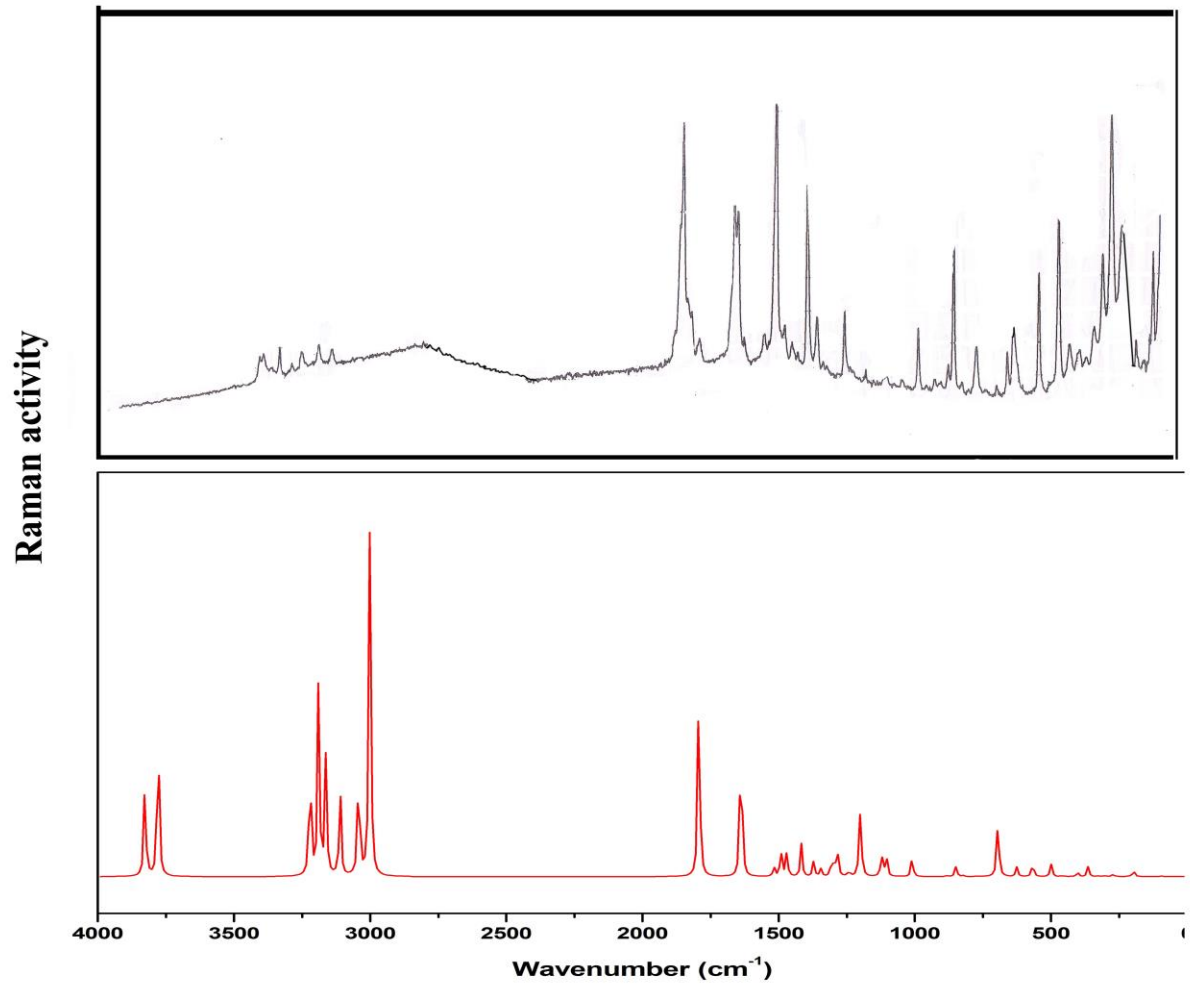
Fig .9
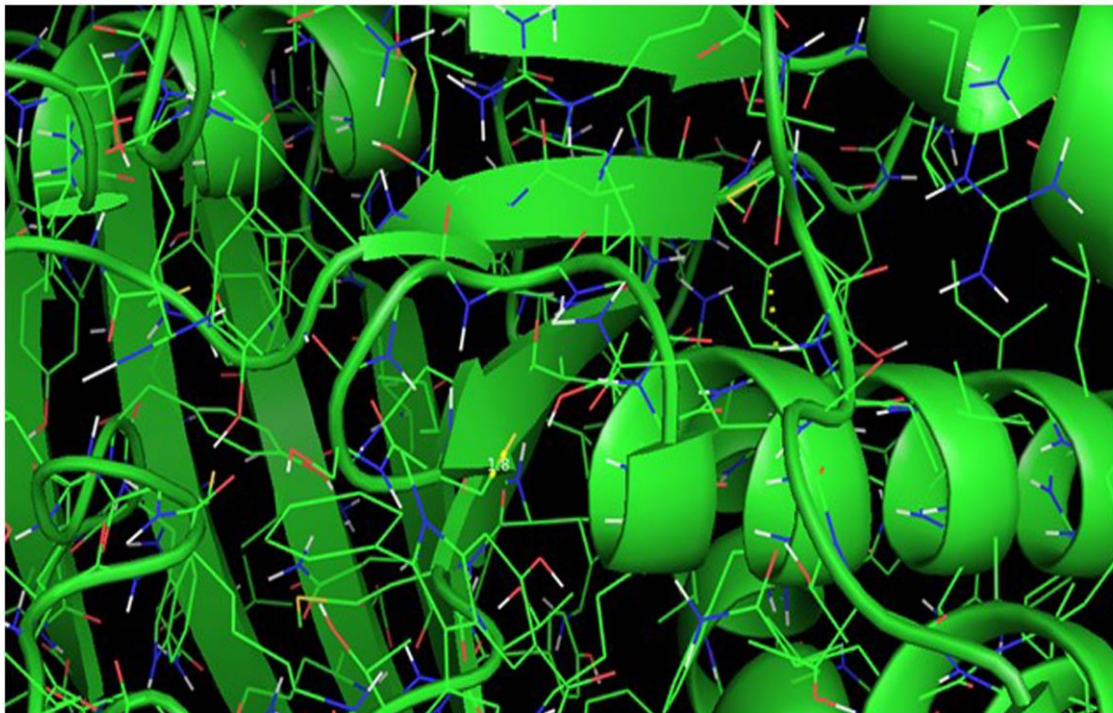
Fig .10

Table 1. Optimized geometrical parameters of 3MESA, bond length (Å) and bond angles (°)

Bond length	B3LYP/ 6-311++G(d,p)	HF/ 6-311++G(d,p)	Bond angle	B3LYP/ 6-311++G(d,p)	HF/ 6-311++G(d,p)
O2-C10	1.3910	1.4299	C4-C7-C9	121.09	122.05
O2-H15	0.9925	0.8531	O2-C10-C6	110.44	112.35
O3-C10	1.2075	1.2583	H15-O2-C10	111.74	112.14
C4-C7	1.3931	1.4013	O3-C10-O2	118.01	119.05
C7-C9	1.4051	1.4013	C7-C9-C8	120.28	121.15
C7-H11	1.0916	1.0698	H11-C 7-C4	119.76	120.25
C9-H13	1.0884	1.0699	H13-C9-C7	119.58	120.58
C16-C4	1.4924	1.5399	C16-C4-C7	121.35	122.21
C16-H17	0.6418	0.3604	H17-C16-C4	129.50	130.70
C16--H18	0.6418	0.3696	H18-C16-H17	69.05	70.35
C16-H19	1.1002	0.9361	H19-C16-H18	118.45	119.78
O1-H14	0.9936	0.8441	H14-O1-C5	112.80	113.63
C8-H12	1.0955	1.0699	H12-C8-C9	120.77	121.58
C9-C8	1.3885	1.4012	C9-C8-C6	120.58	121.38
C5-C6	1.4100	1.4013	C5-C6-C8	118.42	119.15
C8-C6	1.4102	1.4013	O1-C5-C4	122.77	123.13
O1-C5	1.3620	1.4299	C10-C6-C8	120.75	121.58
C10-C6	1.4693	1.53985	C4-C5-C6	120.51	120.47
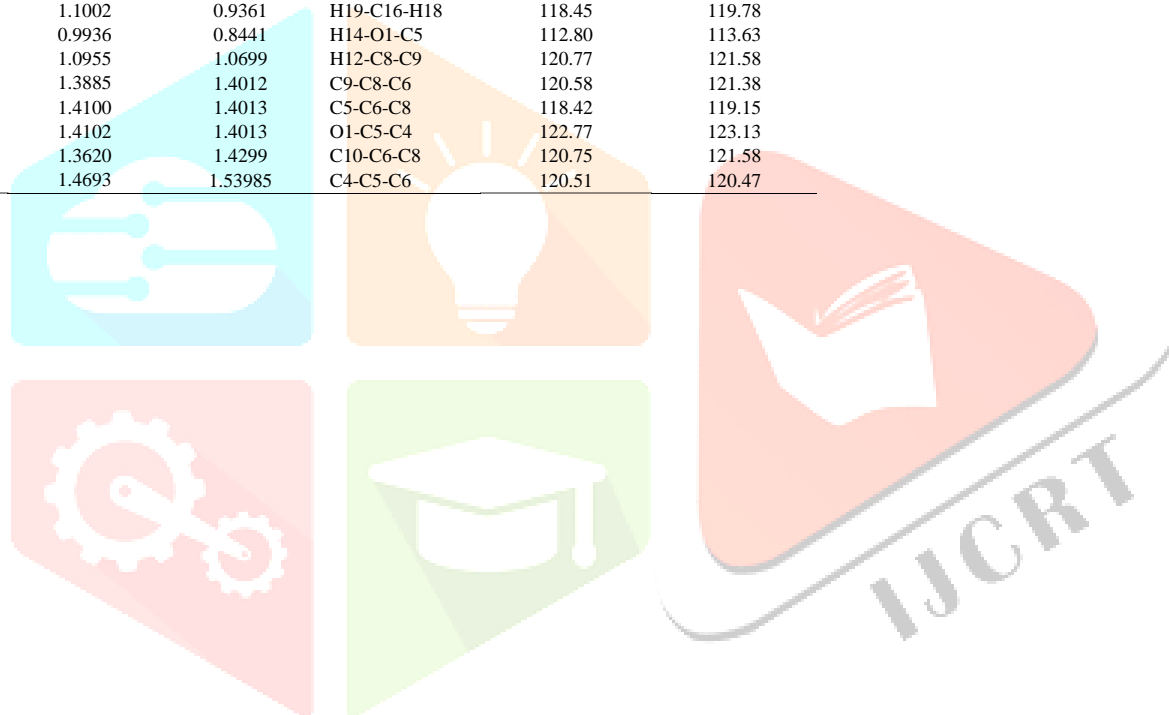
Table 2. Thermodynamic properties at different temperatures at the B3LYP/6-311++G(d,p) level for 3MESA

Temperature	C Heat capacity	S Entropy	H Enthalpy
100	12.119	65.182	0.926
150	19.099	74.752	1.934
200	25.427	83.120	3.062
250	31.668	92.523	5.142
298.15	38.186	98.331	6.386
350	42.419	104.832	8.610
400	46.752	108.126	10.863
450	50.556	111.421	13.117
500	54.300	114.561	15.325
550	57.761	117.575	18.752
600	60.795	120.089	21.786
650	64.610	122.863	25.080
700	67.526	125.755	27.988
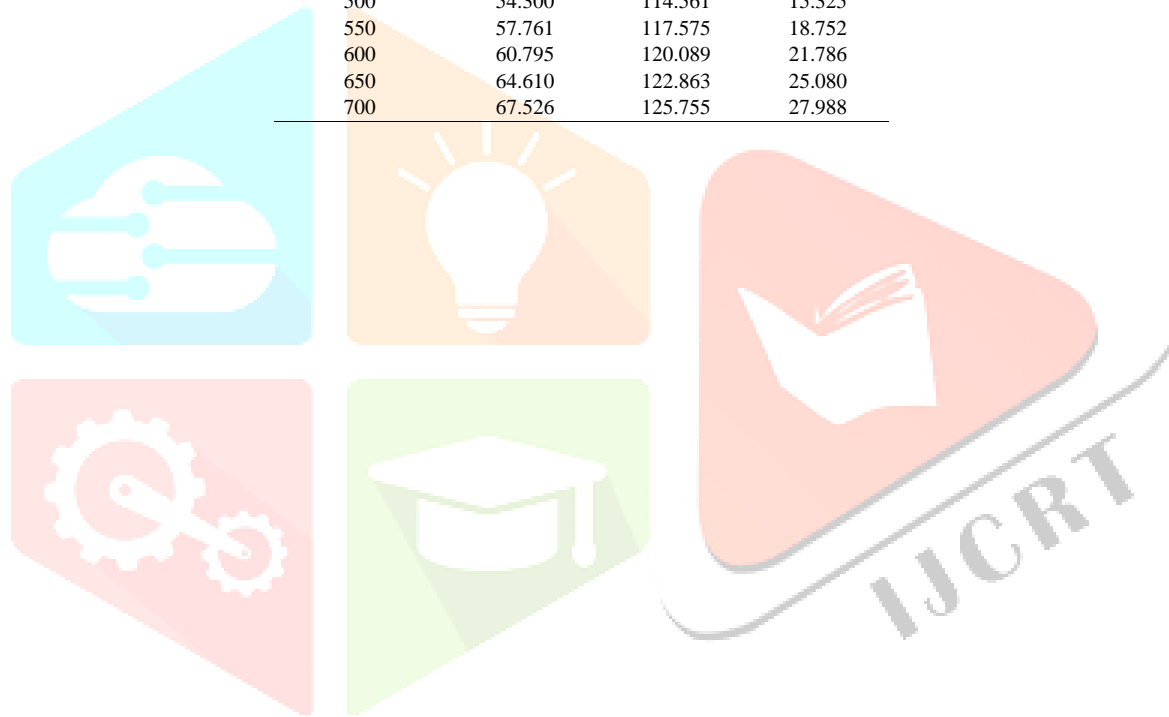
Table 3. Mulliken atomic charges of 3MESA

Atoms	Mulliken charges	
	HF 6-311 ++G(d,p)	B3LYP 6-311 ++G(d,p)
O1	-0.288135	-0.173309
O2	-0.279097	-0.186178
O3	-0.392999	-0.290741
C4	0.766981	0.624257
C5	-0.038923	-0.437538
C6	0.198477	0.169804
C7	-0.483120	-0.226212
C8	-0.731202	-0.500453
C9	-0.504095	-0.487641
C10	0.630878	0.507018
H11	0.164098	0.124602
H12	0.241935	0.196128
H13	0.206976	0.170597
H14	0.317403	0.290686
H15	0.319828	0.289746
C16	-0.635437	-0.573576
H17	0.160305	0.158729
H18	0.160304	0.158727
H19	0.185823	0.185355

Table 4. Calculated energy values, chemical hardness, electro negativity and dipole moment of in Acetonitrle Chloroform, DMSO, Ethanol and gas phase

TD–DFT/B3LYP/ 6–311++G(d,p)	Acetonitrle	Chloroform	DMSO	Ethanol	Gas
E_{total} (Hartree)	-535.5284	-535.5246	-535.5154	-535.5281	-535.5051
E_{HOMO} (eV)	-6.6242	-6.6006	-6.4832	-6.6220	-6.4097
E_{LUMO} (eV)	-1.7242	-1.6729	-1.4940	-1.7201	-1.3334
$\Delta E_{HOMO-LUMO\ gap}$ (eV)	4.9000	4.9277	4.9892	4.9019	-5.0762
E_{HOMO-1} (eV)	-7.3763	-7.3530	-7.2573	-7.3744	-7.1778
E_{LUMO+1} (eV)	-0.4466	-0.4317	-0.2589	-0.4452	-0.2098
$\Delta E_{HOMO-1-LUMO+1\ gap}$ (eV)	6.9298	6.9214	6.9984	6.9292	-6.9679
E_{HOMO-2} (eV)	-7.9242	-7.8087	-7.6753	-7.9155	-7.2952
E_{LUMO+2} (eV)	-0.2703	-0.3104	1.0127	-0.2722	0.5984
$\Delta E_{HOMO-2-LUMO+2\ gap}$ (eV)	7.6538	7.4982	8.6879	7.6433	-7.8936
Electronegativity χ (eV)	4.1742	4.1368	3.9886	4.1711	-6.4097
Chemical hardness η (eV)	2.4500	2.4638	2.4946	2.4510	1.2690
Softness ζ (eV)$^{-1}$	0.2041	0.2029	0.2004	0.2040	-2.5381
Electrophilicity index ψ (eV)	3.5559	3.4728	3.1886	3.5492	3.8751
Dipole moment (Debye)	4.5500	4.2284	4.0268	4.5260	3.0482

Table 5. Theoretical electronic absorption spectra of 3-methyl salicylic acid (absorption wavelength λ (nm), excitation energies E (eV) and oscillator strengths (f)) using TD-DFT/B3LYP/6-311++G(d,p) method in gas and solvent (Acetonitrile, Chloroform, DMSO , Ethanol and Gas) phase.

Acetonitrile	λ (nm)	E (eV)	(f)	Major contribution
	4.2867	289.23	0.1043	HOMO—LUMO(93)
	4.8776	254.16	0.0001	HOMO-2 —LUMO(96)
	5.2280	237.16	0.2042	HOMO-1 —LUMO(86)
	5.6037	221.25	0.0058	HOMO —LUMO+2(96)
	5.9504	208.36	0.0022	HOMO —LUMO+3(87)
Chloroform	4.3060	287.93	0.1126	HOMO—LUMO(93)
	4.8217	257.14	0.0001	HOMO-2 —LUMO(96)
	5.2413	236.55	0.2082	HOMO-1 —LUMO(85)
	5.5410	223.76	0.0055	HOMO —LUMO+2(97)
	5.8995	210.16	0.0035	HOMO —LUMO+3(87)
DMSO	4.3759	283.33	0.1069	HOMO—LUMO(93)
	4.8654	254.83	0.0002	HOMO-2 —LUMO(96)
	5.5359	231.49	0.1749	HOMO-1 —LUMO(83)
	6.1045	203.10	0.4698	HOMO-1 —LUMO(81)
	6.3776	194.41	0.2583	HOMO-1 —LUMO+1(72)
Ethanol	4.2875	289.18	0.1055	HOMO—LUMO(93)
	4.8735	254.41	0.0001	HOMO-2 —LUMO(96)
	5.2279	237.16	0.2059	HOMO-1 —LUMO(83)
	5.5995	221.42	0.0058	HOMO —LUMO+2(97)
	5.9465	208.50	0.0027	HOMO —LUMO+3(87)
Gas	4.1760	296.90	0.0865	HOMO—LUMO(90)
	4.5345	273.42	0.0001	HOMO-2—LUMO(96)
	5.2999	233.94	0.0920	HOMO-1 —LUMO(72)
	5.9619	207.96	0.0019	HOMO —LUMO+2(92)
	6.0058	206.44	0.4290	HOMO-1 —LUMO(91)

Table 6: Experimental (FT-IR and FT-Raman) wavenumbers and detailed assignments of theoretical wavenumbers of along with potential energy distribution of 3MESA

Sl.No	S^y	Infrared	Raman	HF Unscaled	HF scaled	B3LYP Unscaled	B3LYP Scaled	I^{IR}	I^{Ra}	Vibrational assignment
1.	A′			4208	3815	3827	3666	74.51	85.95	γOH(98)
2.	A′	3620 vw		4132	3747	3778	3620	98.07	141.21	γOH(94)
3.	A′		3080 vw	3391	3074	3221	3086	1.77	95.61	γCH(99)
4.	A′			3349	3036	3189	3055	10.59	141.13	γCH(100)
5.	A′		3030 vw	3322	3012	3163	3030	9.41	85.50	γCH(98)
6.	A′	2980 w		3254	2950	3111	2980	9.74	64.83	γCH(99)
7.	A′	2920 w		3190	2892	3042	2915	17.14	88.26	γCH(95)
8.	A′	2870 s		3146	2853	3001	2875	28.75	234.98	γCH(96)
9.	A′	1720 vw		1989	1803	1793	1718	419.48	100.49	γCO(86)
10.	A′	1610 s		1791	1623	1640	1612	60.04	48.32	γCO(85)
11.	A′			1779	1613	1633	1605	20.76	19.38	γCO(89)
12.	A′	1485 m		1638	1485	1517	1491	6.92	4.28	γCC(89)+ γCO(19
13.	A′	1470 m		1619	1468	1496	1471	19.67	2.59	γCC(81)+ γCO(16)
14.	A′			1609	1459	1489	1464	8.78	9.65	γCC(85)+γCO(12)
15.	A′	1440 m		1591	1443	1469	1444	76.68	12.16	γCC(78)
16.	A′	1390 vw		1540	1396	1417	1393	12.64	15.49	γCC(74)
17.	A′	1336 w		1478	1340	1372	1348	44.37	6.84	γCC(81)
18.	A′		1325 w	1434	1300	1346	1323	72.52	3.47	γCC(68)
19.	A′	1295 vs		1404	1273	1304	1282	35.85	9.52	γCC(62)
20.	A′	1260 vw		1361	1234	1285	1263	28.88	16.11	βOH(64)+ γCC(18)
21.	A′	1225 vs		1312	1190	1242	1221	53.35	2.79	βOH(66))+ γCC(13)
22.	A′	1175 s		1299	1178	1202	1181	183.50	27.84	βCH(61))+ γCC(10)
23.	A′	1168 vs		1263	1146	1191	1171	1.33	3.73	βCH(64))+ γCC(12)
24.	A′		1105 vw	1217	1103	1122	1103	90.18	9.80	βCH(62))+ γCC(14)
25.	A′	1090 w		1180	1070	1105	1086	253.04	10.47	βCH(68)
26.	A′	1040 vw		1158	1050	1057	1039	0.84	0.09	βCH(64)+ γCC(18)
27.	A′	1005 vw		1106	1003	1010	993	2.16	8.55	βOH(62)
28.	A′		965 vw	1085	983	988	972	0.28	0.00	βCH(63)
29.	A′	905 vw		1058	959	938	922	0.16	0.03	βCO(66)
30.	A′	862 vw		945	856	882	867	29.13	0.63	βCO(65)
31.	A′	830 vw		917	831	848	834	13.20	4.54	βCO(66)
32.	A″			909	824	823	809	0.32	0.37	φOH(63)
33.	A″	750 vs		852	772	769	756	77.04	0.10	φOH(51) + βCCC(13)

Table 7. Second order perturbation theory analysis of Fock matrix in NBO basis for 3MESA

Donor (i)	Type of bond	Occupancy	Acceptor (j)	Type of bond	Occupancy	E2 (kJ mol−1)[a]	E(j) −E(i) (a.u.)[b]	F(i, j) (a.u.)[c]
O1-C5	σ	1.99367	C 4-C5	σ*	0.03754	1.26	1.45	0.038
			C4-C7	σ*	0.01651	1.42	1.50	0.041
			C5-C6	σ*	0.03069	0.88	1.47	0.032
			C6-C8	σ*	0.02023	1.79	1.48	0.046
O2-C10	σ	1.99483	C5-C6	σ*	0.02023	2.08	1.42	0.049
O3-C10	σ	1.99573	C6-C8	σ*	0.06272	1.03	1.62	0.037
			C6-C10	σ*	0.01704	2.93	1.52	0.060
			C5-C6	σ*	0.03754	3.73	0.39	0.038
C4-C5	σ	1.97289	C 4-C7	σ*	0.01651	3.79	1.28	0.062
			C4-C16	σ*	0.03069	2.06	1.12	0.043
			C5-C6	σ*	0.06272	4.73	1.24	0.068
			C6-C10	σ*	0.01442	2.52	1.14	0.048
			C7-H11	σ*	0.00599	2.52	1.12	0.048
			C16-H19	σ*	0.02013	0.89	1.08	0.028
C4-C7	σ	1.97139	O1-C5	σ*	0.03754	3.82	1.05	0.057
			C4-C5	σ*	0.01651	3.72	1.23	0.061
			C4-C16	σ*	0.01623	2.86	1.12	0.051
			C7-C9	σ*	0.01442	3.16	1.27	0.057
			C7-H11	σ*	0.03754	1.03	1.13	0.031
			C9-H13	σ*	0.01433	2.05	1.14	0.043
C4-C7	π	1.68908	C5-C6	π*	0.42023	23.33	0.28	0.074
			C8-C9	π*	0.29980	16.17	0.29	0.062
			C16-H17	π*	0.01213	3.38	0.63	0.045
			C16-H18	π*	0.01213	3.38	0.63	0.045
C4-C16	σ	1.97949	C4-C5	σ*	0.01651	2.22	1.18	0.046
			C4-C7	σ*	0.01651	3.00	1.23	0.054